Tribology International 180 (2023) 108308

Contents lists available at ScienceDirect

Tribology International

journal homepage: www.elsevier.com/locate/triboint

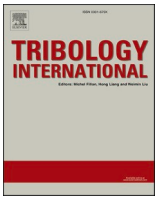

Novel paradigm in AFM probe fabrication: Broadened range of stiffness, materials, and tip shapes

Michał Milczarek [a], Dariusz M. Jarząbek [a,b,*], Piotr Jenczyk [a], Kamil Bochenek [a], Maciej Filipiak [c]

[a] Institute of Fundamental Technological Research, Polish Academy of Sciences, Pawińskiego 5B, 02-106 Warsaw, Poland
[b] Warsaw University of Technology, Faculty of Mechatronics, Institute of Micromechanics and Photonics, Boboli 8, 02-525 Warsaw, Poland
[c] Centre for Advanced Materials and Technologies CEZAMAT, Warsaw University of Technology, Poleczki 19, 02-822 Warsaw, Poland

ARTICLE INFO

Keywords:
Atomic force microscopy
Microfabrication
Cantilever
Metal probe
Friction
Nanotribology

ABSTRACT

Atomic force microscopes could be used in wide range of nanotribology experiments but probes available on the market are only made of silicon or silicon nitride with a stiffness in the range of 0.01–100 N/m, which significantly limits the possible research. We strive to solve this problem by designing all-metal probes. The proposed fabrication method is characterised by the use of a copper substrate and electrodeposition in a mould prepared by indentation and photolithography. Prototype probes fabricated with this method were made of nickel with a stiffness of 20 N/m and 2800 N/m and were used for topography and friction measurements. Both the method and all-metal probes showed flexibility and great potential, especially in the field of nano/microtribology.

1. Introduction

Atomic force microscopes (AFM) are one of the most popular tools used for micro- and nanoscale research. Since the invention of AFM in 1986 [1], their popularity has been growing. During the past several years, a great number of papers about new techniques, new probes, and improvements to hardware and software have been published. AFMs are most commonly used to measure the sample surface topography, but other numerous sample characteristics can be investigated, including electrical, magnetic, thermal, and tribo-mechanical properties [2,3]. For the latter, the most common are hardness, friction coefficient, wear resistance, Young's modulus, and adhesion. Investigation of the mechanical parameters presents unique challenges, as results are heavily dependent on the properties of the AFM probe, such as stiffness and material. Extension of the capabilities of AFM in material research would be particularly useful in the further development of micro/-nanotribology of MEMS [4–6] (micro-electro-mechanical systems) devices or triboelectric generators in which mechanical interactions are crucial for their operation [7–9]. Unfortunately, there is still a big gap in experimental tribology on the boundary between the nano- and microscale caused by a limited selection of tools for such measurements. Firstly, conducting an experiment with any chosen friction pair is challenging since the commercially available probes are usually made of silicon or silicon nitride. The use of a probe made entirely of any other material is problematic and a common solution is to attach a tip from a different material to a silicon cantilever [10] or to modify an existing tip [11,12]. In both cases, expensive Focused Ion Beam (FIB) is used, and the tip-cantilever bond and the fragility of cantilevers are still an issue. Additionally, the range of probes stiffnesses is limited, hence, normal loads possible to apply are usually between a tenth of nanonewtons up to several micronewtons. Milinewtons can be obtained but this requires a special approach [13] that can reduce the measurement sensitivity.

Moreover, other sophisticated AFM experiments also require modified or functionalized probes. For example, the measurement of electrical parameters requires conductive probes, and the measurement of magneticity requires magnetic probes [3]. These properties are typically achieved by coating tips or whole probes with thin layers of metals. These layers provide the required properties, but they simultaneously increase the tip radius, which decreases the imaging resolution. Another disadvantage of such coatings is their fragility. Thin layers can be easily damaged in contact modes, especially during the measurement of friction or wear [14]. Hence, coatings in current use do not sufficiently fulfil the requirements especially of tribological research. All this problems could be solved by manufacturing all-metal probes.

Methods of fabricating metal AFM probes already described in the literature can be divided into two categories – modifications of silicon probes and the creation of all-metal probes. Therefore, silicon probes are modified by incorporating metal tips to improve their different

* Corresponding author at: Institute of Fundamental Technological Research, Polish Academy of Sciences, Pawińskiego 5B, 02-106 Warsaw, Poland.
E-mail address: djarz@ippt.pan.pl (D.M. Jarząbek).

https://doi.org/10.1016/j.triboint.2023.108308
Received 23 December 2022; Received in revised form 24 January 2023; Accepted 27 January 2023
Available online 31 January 2023
0301-679X/

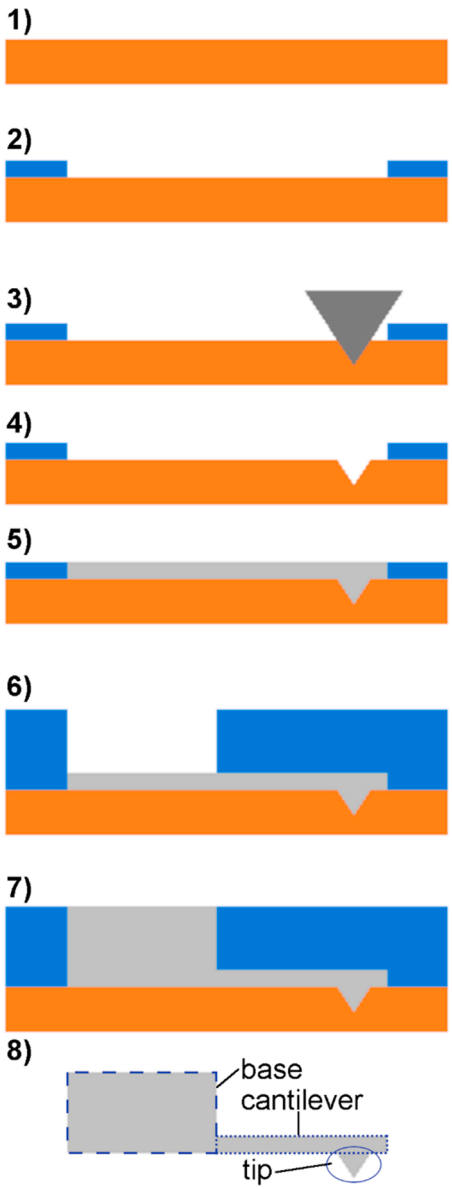

Fig. 1. Fabrication process. Consecutive steps of the method are schematically shown. colour should be used in print.

characteristics. For example, Cespedes [12] used localised electrodeposition of nickel on a previously prepared tip to achieve a high volume of magnetic material to improve magnetic force microscopy. A number of other authors fabricated nanowires at the end of the tip to increase the imaging resolution of the probe and the aspect ratio of the tip. Akiyama et al. [15] used a FIB to etch and sharpen a tungsten nanowire glued to a silicon probe. Tay and Thong [16] developed a method of growing a single nanowire at the tip end using the field emission growth technique. Walke et al. [17] attached chemically grown silver nanowires to the end of the silicon cantilever. These probes, although having some advantages over silicon probes, are not useful for tribological experiments, as the measuring tip is too flimsy for imaging in the lateral mode and would be damaged in a short time.

On the other hand, the probes from the second group are made completely (at least the tip and the beam) of metal. For instance, Michałowski and Łuczak [18] developed probes made of beryllium copper with a submillimeter metal ball attached as a tip. They have been designed specifically for friction measurements between different friction pairs. Unfortunately, their method does not allow full control of probe geometry and possible stiffnesses are relatively high. On the other hand, the probe can also be manufactured from a gold wire [19,20] due to the exceptional ductility of gold. The wire can be bent at one end to form a tip and flattened at the other end to form a beam. It should be noted that many other methods share a lot of similarities [21–23]. In all of them, a silicon substrate is used, in which a pyramid-like mould for a tip is etched. Next, a sacrificial layer is sputtered and then the main layer of the probe material is plated using sputtering or electrochemical deposition. Probes fabricated by these methods are usable in tribological experiments. Unfortunately, the methods alone have important drawbacks – they use costly and complicated procedures (plasma vapour deposition (PVD), precise silicon etching). Moreover, the number of obtainable tip shapes is limited mainly to balls glued to a cantilever or a pyramid resulting from silicon etching.

This paper introduces a new, groundbreaking method of fabricating all-metal probes in which the number of steps and different processes is significantly reduced. Two features distinguish the novel method from the others. The first is the use of a metal substrate that allows direct electrodeposition of the probe material without any sacrificial layer. The second is the possibility of creating any convex tip shape due to the production of a mould for the tip by indentation. These innovations allow a relatively cheap production of all-metal probes with almost any geometry, adapted to the requirements of particular measurements. In this paper, the method is described in detail and probes with various stiffness are fabricated. The manufactured probes are then characterised and used in example tribological experiments. The coefficient of friction between various materials with a normal load on the micro-scale boundary was properly measured. Finally, the advantages and disadvantages of the method are discussed.

2. Experimental

To avoid any misunderstanding caused by differences in the nomenclature used, in this paper names will be defined as follows. The AFM probe consists of three subparts: base, cantilever (beam), and tip. They are marked in Fig. 1 (part 8). The base is a thick, stiff part that is grabbed by tweezers and is mounted in a probe holder. The cantilever or beam is the part that defines the stiffness of the probe and is deformed during the measurement. The tip is the part that interacts with the imaged sample.

The novel method of fabricating all-metal AFM probes is described in detail below, first for all-metal probes and then for probes with microballs as a measuring tip.

2.1. General process for all-metal probes

The illustration of the fabrication steps is shown in Fig. 1. The steps are shown as a cross-sectional side view. The entire method can be divided into seven main parts: substrate preparation (1), beam mould preparation (2), tip mould preparation (3–4), beam and tip material electrodeposition (5), base mould preparation (6), base material electrodeposition (7), and probe release (8).

Metal compatible with subsequent processes is selected as a material for the substrate (1). It must be mechanically polished to a mirror finish, as the roughness of the substrate will greatly influence the surface quality of the fabricated probes.

In step 2, photolithography is used to create a resist-mould defining shape of the beam, base, and all the supporting structures. A negative resist is preferably used, as it allows vertical sidewalls of the structures.

In step 3, the mould for the tip is created with the diamond indenter, normally used for hardness tests. Step 4 in Fig. 1 shows the result of the previous step.

Step 5 is the electrodeposition of the selected material to form the beam and tip. The flexibility of electroplating allows a wide variety of metals to be plated. The bath solution and plating parameters should be chosen to create as smooth a surface as possible and also to limit internal

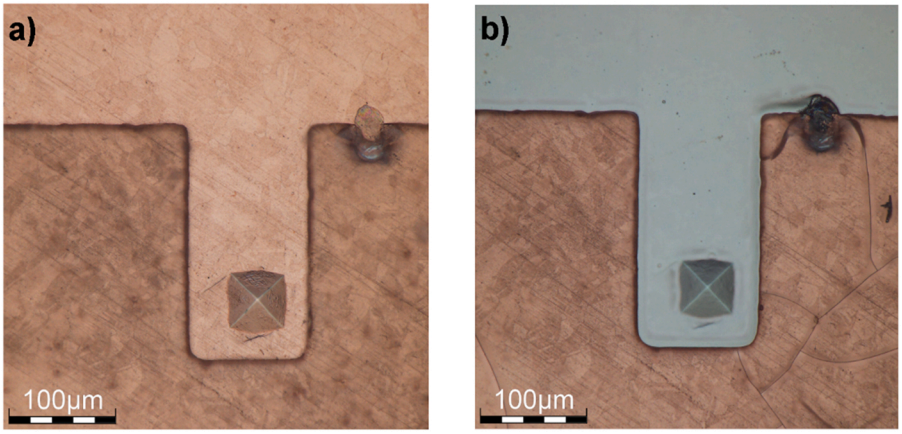

Fig. 2. Optical microscope images of selected steps of the method. Imperfection visible on the right hand side is a result of mould damaged by indentation tip. a) a tip mould after the 4th step, b) the first layer of nickel after the 5th step colour should be used in print.

stresses in the created probes.

Step 6 is the second photolithography process to create a mould for a thick probe base. The resist thickness obtained in this step should be at least 10% higher than the planned thickness of the probe base.

Step 7 is the second electrodeposition to form the probe base. Our experience shows that the base should be at least 200 µm thick to allow easy manipulation with tweezers. For comparison, commercial silicon probes have 315 µm or 500 µm thick bases [24–26]. The same material as in the first plating is recommended, although different materials can be beneficial depending on the purpose of the probes.

To obtain the probe shown in step 8, the unwanted resist and the substrate material must be removed. The resist should be removed with a compatible remover. The substrate should be chemically etched with a solution with high selectivity towards that specific material to ensure that the probe will not get damaged.

The final result of the described process are probes interconnected with supporting structures. The probes can be easily removed with the help of tweezers and are ready for use in AFM.

2.1.1. Details of the fabrication

All the processes were conducted two times, first to obtain soft probes (with 10 µm thick beams) and second to obtain stiff probes (with 40 µm thick beams).

Technical grade pure copper was used as a substrate. Copper is a soft metal, therefore it will be easy to create indentations (moulds for tips) and it will lead to slow wear of indentation tip. Copper can also be selectively etched with various other metals (for example selectively to silver by $FeCl_3$ [27]). Technical purity is enough as it will be completely lost and serves only as a substrate. Disks with a diameter of 51 mm (2 in.) were cut from the 0.5 mm thick sheet. One side of the disk was polished to a mirror finish with surface roughness parameter S_a at about 5 nm. All the subsequent steps of the process were conducted on the polished side of the substrate.

For the photolithography resist, AZ 125nXT supplied by MicroChemicals GmbH was used. It was dispersed on the substrate for 15 s at a speed of 5000 rpm (13 µm layer), 1000 rpm (80 µm layer), or 800 rpm (100 µm layer). Soft bake was performed on a hot plate at 120 °C for 15 min. For super thick 200 µm layers, the process was repeated 2 times. Parameters were taken from documentation provided by the resist manufacturer with minor changes tailoring the process to devices available in the laboratory.

The exposure was performed on the EVG6200NT mask aligner in the broadband mode. The dose was set at 500 mJ/cm^2 (13 µm layer), 2500 mJ/cm^2 (80 µm layer), and 6000 mJ/cm^2 (200 µm layer). The exposure was conducted in a soft contact mode through a foil mask manufactured by a local printing company in CTF (computer to film) technology. The resist was developed for 3–6 min in AZ 726 MIF developer supplied by MicroChemicals GmbH. Parameters were taken from documentation provided by the resist manufacturer with minor changes tailoring the process to devices available in the laboratory.

The tip mould was prepared with a micro indentation tester from Anton Paar. A diamond Vickers indenter tip was used, which has the shape of a 4-sided pyramid with a tip angle of 136°. Indentation was conducted with constant load and resulting indentation depth (and tip-mould depth, and later tip height) was around 8 µm. The substrate after this step is shown in Fig. 2a.

Nanocrystalline nickel was selected as the material for electroplating. The bath used for this process was a modified Watts bath. Additives such as saccharin and potassium chloride were used to minimise internal stresses in a plated layer [28,29]. A plating solution should be chosen, whether self-made or off-the-shelf, to create a bright deposit.

During electroplating, the polished copper substrate was used as a cathode and the anode was made of a technical-grade pure nickel rod. The temperature of the solution was maintained within the range of 55–60 °C by the hotplate with a closed-loop control. Agitation of the bath was achieved by using a magnetic stirring rod at a speed of 200 rpm. Directly before plating, the pH was set to 4 by adding diluted NaOH or HCl. The current density was set at 1.8 A/dm^2. Control of the bath parameters is crucial to create a flat surface and recreating the smoothness of the polished substrate. Therefore parameters should be closely recreated from documentation provided by the manufacturer, paper of other scientists, or set by own experiments to create a bright and stress-free layer. The plating lasted 15 min, 55 min, and 350 min for first layer of soft probes, first layer of stiff probes, and bases, respectively, resulting in thicknesses of 10 µm, 35 µm, and 220 µm, respectively. An example of the mould after the first electrodeposition is shown in Fig. 2b.

The resist was removed with TechniStrip P1316 supplied by MicroChemicals GmbH. The sample was put in a remover heated to 70 °C for 10 min. Then, two consecutive baths were performed to ensure the removal of all the residual resist. The copper substrate was fully removed with a selective etching solution. No deterioration in the tip sharpness was observed.

2.2. Probes with balls as tips

Using balls as the measuring tip of a probe is beneficial for tribological experiments, as it allows direct comparisons with macro-scale experiments by closely recreating experimental setup at smaller scale. It is also convenient to use spheres in the modelling of contact and validation of such models [30–32]. Moreover, micro-balls made from a wide variety of materials are available on the market. Our metal probes

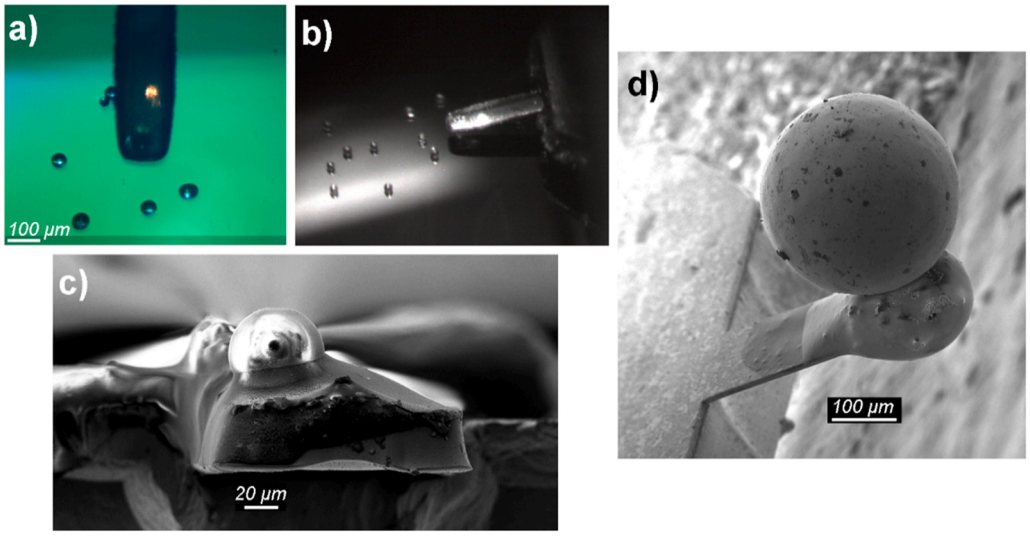

Fig. 3. Attaching balls to metal cantilever, a) top view from AFM camera, b) side view from AFM camera, c) SEM image of the probe with ball, d) another probe with a sphere with a diameter of 300 µm colour should be used in print.

have an advantage over the classical silicon probes as a base for gluing balls. With the same stiffness, metal probes are larger; therefore, they are easier to manipulate and are more durable. It is then easier to use adhesives without destroying the probe.

To showcase the flexibility and usefulness of probes fabricated with method described above, stiff probes with glass balls as a tip were produced. The procedure was conducted as follows. The balls were soda-lime glass microspheres with a diameter of 41 µm (± 3 µm) obtained from Cospheric LLC. Two-component epoxy with a curing time of 10 min was used as an adhesive. The balls were dispersed on the surface of the silicon wafer, and a drop of mixed epoxy was placed nearby. The microscope head allowed for vertical (Z-axis) motion, while the sample stage provided horizontal motion (X- and Y-axis). Firstly, the cantilever of the probe was positioned above the drop of glue and dipped in it. Then, it was moved above the empty silicon surface and touched it to remove excess epoxy. Lastly, the cantilever of the probe was moved above a single ball (Fig. 3a and b), lowered to make contact with the ball and left in contact for approximately 1 min to bond the ball to the beam, and then lifted as one. After an additional 10 min of curing the epoxy, the probe was ready to be used for measurements. A close-up picture of

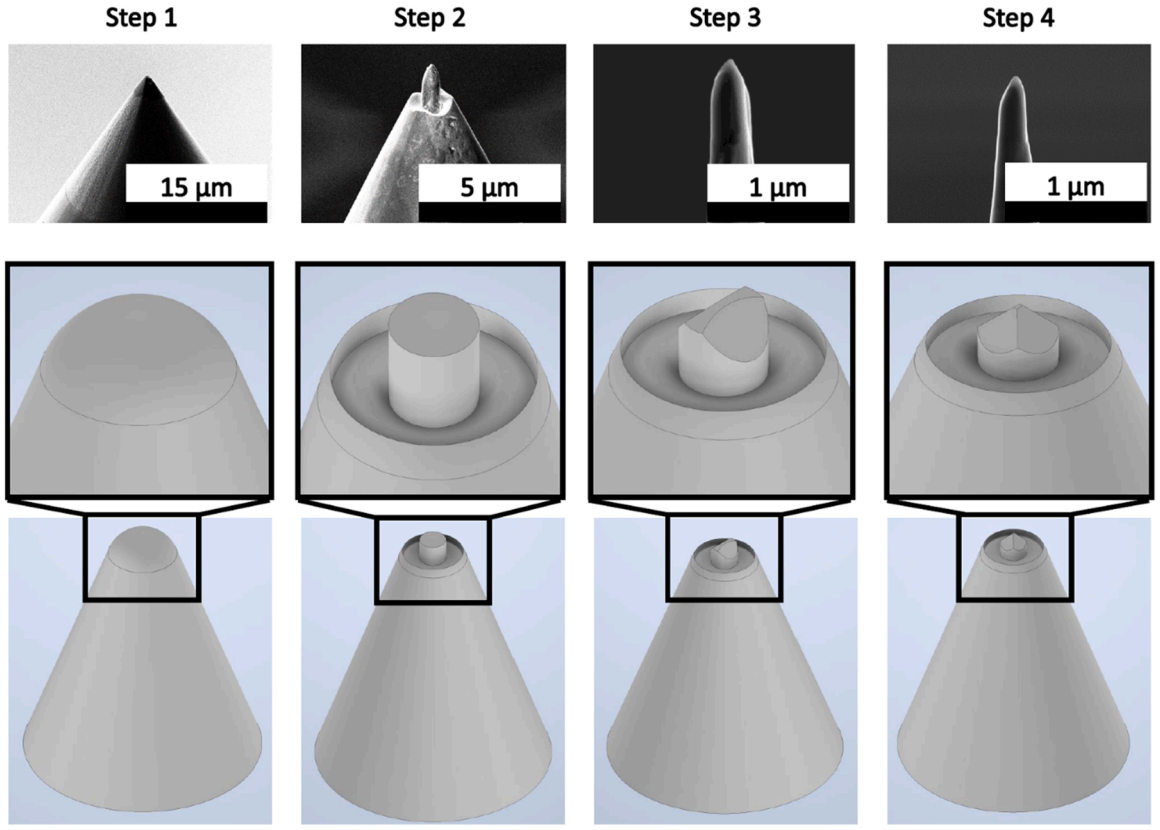

Fig. 4. FIB milling process – creating high-aspect-ratio tip from conical indenter.

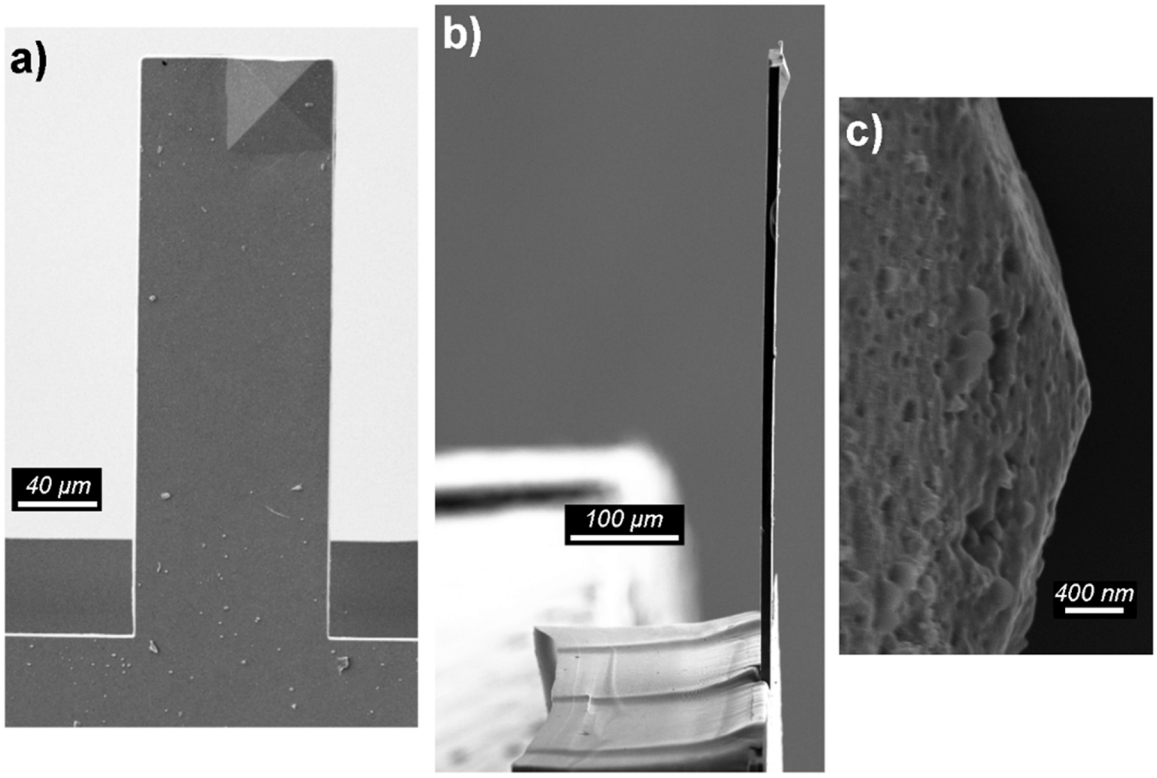

Fig. 5. SEM images of the probe, a) cantilever with dimensions, b) side view of the probe, c) close-up of the tip.

the ball-tip is shown in Fig. 3c. Note that the image is slightly warped due to the charging of a non-conductive ball.

Additionally, a 300 μm sphere was attached to a probe designed for different kind of experiment, which fall outside of the scope of this paper but the probe is shown as an example of the advantages of metal probes over silicon probes. It was prepared as described above with the only difference being the amount of glue at the cantilever. This probe is shown in Fig. 3d) and a big lump of epoxy is visible at the end of the cantilever, the cantilever has dimensions of 440 μm x 145 μm x 10 μm.

2.3. Probe characterisation methods

Numerous tools and methods were used in the characterisation of the probes. The size and shape of the manufactured probes were investigated by an optical microscope (OM) Olympus DSX500 and a scanning electron microscope (SEM) Zeiss Crossbeam 350. The atomic force microscope used for the experiments was the Nanosurf FlexAFM.

The normal stiffness of the probe is a crucial parameter for tribological experiments; therefore, significant attention was given to proper determination of this parameter. Three methods can be used: geometrical [33], indirect from resonant frequency [34], and direct with the help of a nanoindenter [35]. Described of all the methods is given in Appendix 1. Our experiments showed that the best results are obtained from the direct method. It had the lowest uncertainty and takes into account all the imperfections of a probe that are omitted in calculations. Therefore, it was used for calibration in this paper.

Additionally, the lateral force calibration constant (LFCC), which directly relates the lateral signal from AFM with the force on the end of the tip, was determined using a previously developed method [36]. It uses an ultra-precise device with a MEMS force-sensor on which the AFM-tip is positioned and moved in the lateral mode. As the calibration is done directly in AFM, it takes into account all parts of the system (probe shape and torsional stiffness, AFM detector sensitivity) and allows for a greater precision than the other methods. The authors reported an uncertainty of 3%, and this value is assumed in the calculations in this paper. For calibration of the thick probe force sensor in the calibration device had to be changed for stiffer, more rigid, and therefore less precise, which increased the uncertainty to 5%.

2.4. Custom tip shapes

Our novel approach allows for any convex shape of the probe tip to be easily produced. To showcase this feature, a small batch of tips with different shapes was created. Firstly, a commercial cube-corner indentation tip (supplier – Synton-MDP, Switzerland) was used and secondly a custom indentation tip with a high aspect ratio was created by FIB-milling a commercial conical indenter (supplier – Synton-MDP, Switzerland).

The custom tip was prepared by FIB milling. All steps of the process are shown in Fig. 4, both as a schematic and the actual milled tip. Diamond with the shape of a cone with a 60° apex angle and a tip radius of 1 μm was used as a base for treatment (step 1). Firstly, rough milling was done axially, looking from the apex, and the material was removed in the shape of a ring (step 2). After this step, a thin (0.5–1.5 μm in diameter) and long (around 4 μm) pillar was obtained. In the second step, milling was done perpendicular to the axis of the pillar and only at the apex (step 3). The purpose of this step was to precisely remove the material to form a sharp tip. Lastly, the pillar was rotated 90° around its axis to repeat the precise milling (step 4). The resulting indentation tip had a radius of curvature of 45 nm.

The described indentation tips were used to make a mould in the copper substrate with the help of an Alemnis indenter. The substrate (and moulds) was then covered with nickel by electroplating, and then the substrate was chemically removed.

2.5. Determination of coefficient of friction (COF)

The coefficient of friction (COF) is one of the crucial parameters of two bodies in contact and in motion relative to each other [37,38]. Detailed description of COF determination with the use of AFM was

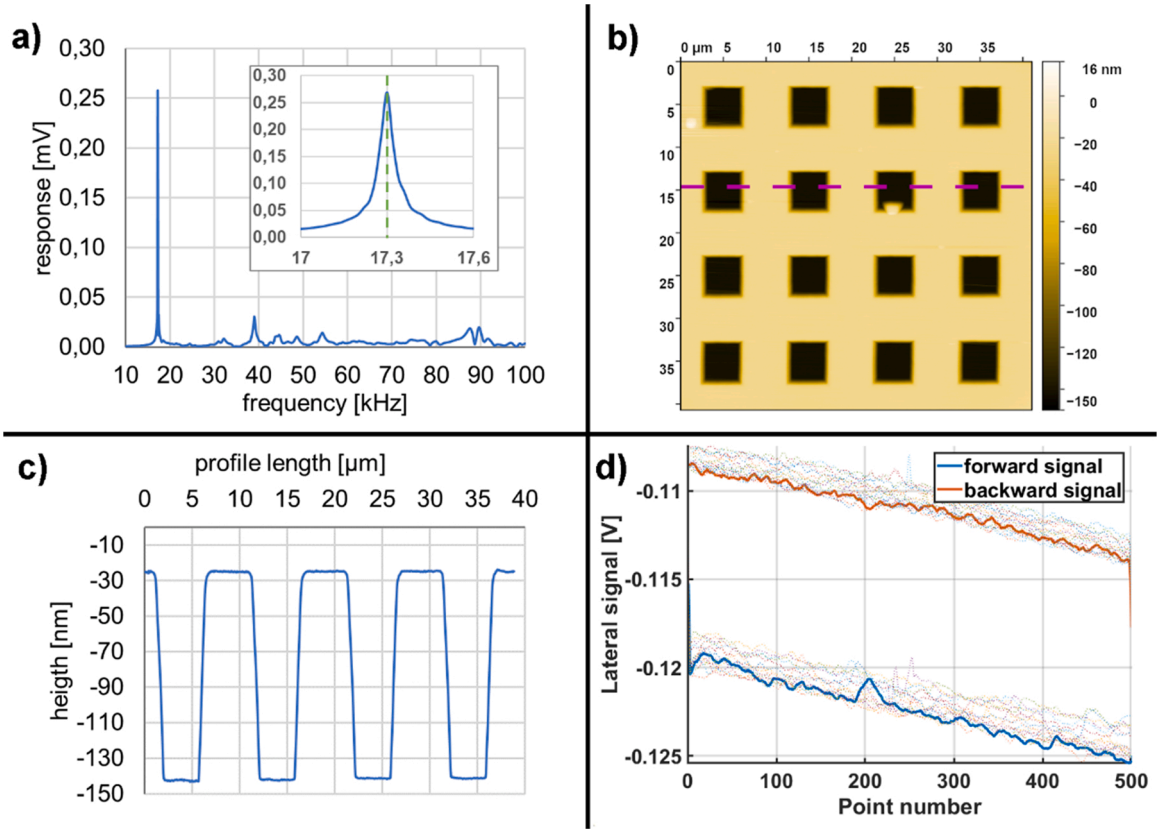

Fig. 6. Results obtained with nickel probe, a) frequency response of cantilever, b) topography image of calibration sample (with marked profile), c) profile extracted from topography image, d) friction loop on a silicon wafer colour should be used in print.

given in a previous paper [39] and here is presented just a synopsis with the most important formulas. Basically, COF is defined as follows:

$$COF = \frac{F_F}{F_N} \tag{1}$$

in which: F_F – friction force [N], F_N – normal force [N].

The formula used to calculate friction force F_F from data obtained with an AFM is given below:

$$F_F = LS \bullet LFCC \tag{2}$$

in which: LS – lateral signal [V], $LFCC$ – Lateral Force Calibration Constant [N/V].

In the above equation lateral signal is measured by the AFM and the LFCC is determined as described in paragraph 2.3.

The formula used to calculate normal force F_N from data obtained with an AFM is given below:

$$F_N = k \bullet s \bullet SP \tag{3}$$

in which: k – normal stiffness of cantilever [N/m], s – sensitivity of AFM diode [m/V], SP – setpoint [V].

In the above equation, normal stiffness is determined as described in paragraph 2.3 and a setpoint is given in the AFM software by its operator. The sensitivity of the AFM system (mainly photodiode) is not the property of the probe and it is determined directly before the measurement by the force-distance curve. A probe is pressed against hard substrate (sapphire crystal) and its deflection is measured. The ratio of the measured deflection to measured movement in Z-axis is then given as sensitivity in m/V.

3. Results

The probes fabricated and characterised with the methods described above were used in actual tribological experiments. Below, details on the results of their inspection, calibration, and testing is given. All-metal probes were used in topography imaging and also to determine the coefficient of friction on silicon, nickel, and copper. A stiff probe with a ball-tip was used for friction experiments on silicon, steel, titanium, and titanium carbide (TiC).

3.1. All-metal probe testing

With the help of the OM and SEM, the appearance of the probes and their actual dimensions were investigated. The top surface of the base was rough and not perfectly flat; however, this was expected as a result of the long electrodeposition. The surface of the cantilever beam was flat and smooth, and its dimensions were in the range of error of the printed mask (shown in Fig. 5a). The sidewalls of the probes were perpendicular to the top and bottom (shown in Fig. 5b). The dimensions of the beam used later in the experiments were measured to be 105 µm x 590 µm x 10.4 µm (width x length x thickness). Bending of the cantilever caused by internal stresses was negligible, as it was barely visible. The deposited material recreates the substrate surface and has a constant thickness; therefore, it creates a recess on the top surface of the beam above the tip mould (example in Fig. 2b). This limits the area on which the laser can be positioned in the microscope but does not influence the working principle of the probe. Due to the use of a standard Vickers indenter, which was previously used for other experiments, the radius of the tip end was relatively large. The measured radius was 350 nm (shown in Fig. 5c); nonetheless, the shape of the indenter tip was precisely recreated.

The inspected probe was then calibrated and used in real-life

Table 1
Results of the friction coefficient measurement with the all-metal probe.

	Substrate type		
	Silicon	Nickel	Copper
Ra roughness [nm]	0.75	45.76	11.43
Nickel probe, 10 μN load, COF:	0.215 ± 0.021	0.293 ± 0.024	0.287 ± 0.024
Silicon probe, 10 μN load, COF:	0.124 ± 0.008	0.176 ± 0.026	0.152 ± 0.040
Nickel probe, 20 μN load, COF:	0.152 ± 0.012	0.241 ± 0.014	0.236 ± 0.014
Silicon probe, 20 μN load, COF:	0.133 ± 0.008	0.129 ± 0.021	0.125 ± 0.011
Nickel probe, 50 μN load, COF:	0.127 ± 0.014	0.219 ± 0.013	0.230 ± 0.012
Silicon probe, 50 μN load, COF:	0.193 ± 0.011	0.217 ± 0.076	0.814 ± 0.054

imaging in AFM. It was mounted in the microscope, and the laser was positioned close to the centre point of the cantilever. The strength of the signal from the reflected beam was at the level of 18% (for a typical Si probe, it is 30%, while the operable minimum is 8%), as reported by the AFM software. Then, the "sensitivity" (or diode calibration constant) was determined by force curves performed on a sapphire substrate. The calculated sensitivity was 720 nm/V. Afterwards, a frequency response of the probe was investigated in the range of 10–100 kHz, and the obtained graph is shown in Fig. 6a (with the inlet showcasing a 17–17.6 kHz range). The resonant frequency was determined to be 17.3 kHz, while the frequency calculated from the dimensions of the probe was 23 kHz. Direct calibration of the normal stiffness with the nanoindentation tester gave the value of 20.88 ± 1.36 N/m.

The calibrated probe was used to image the calibration sample in the contact mode. The obtained image is shown in Fig. 6b. The imaged sample was an HS-100MG grid manufactured by BudgetSensors. From this image, a single profile was extracted to better showcase the shape of the edges (Fig. 6c). Additionally, a measurement in the lateral force mode was performed on a silicon wafer, and a single friction loop extracted from it is shown in Fig. 6d, with other loops shown in the background.

3.2. Friction with the all-metal probe

The probe described in the previous paragraphs was used for the measurement of friction on three different samples: silicon wafer, nickel, and copper. The roughness of the samples was measured on 20 μm long profiles extracted from a levelled image. The coefficient of friction (COF) was measured using the lateral force mode. A single line of measurement was 20 μm long, and the speed of the tip was 20 μm/s. The normal force was set at 10, 20, and 50 μN. 20 lines were obtained in a single experiment. For the probe used in the experiment, the LFCC was 0.887 mN/V.

Additionally, the same measurements were repeated with a commercially available silicon probe – NCL from Nano World, Switzerland. It had a stiffness of 46 N/m and LFCC was 0.061 mN/V. Tip radius curvature less than 8 nm, as declared by manufacturer.

The results of both the roughness and friction are shown in Table 1. The uncertainty of the results is calculated as a combination of the uncertainty of the determination of the probe parameters and the standard deviation of the obtained results.

3.3. Stiff probe with the ball as the tip – characterisation and testing

A stiff probe with a glass ball as the tip was characterised similarly to an all-metal probe. The appearance of the probe and its actual dimensions were investigated with the help of the OM and SEM. The bottom of the beam was perfectly flat with sidewalls perpendicular to it. The surface of the cantilever beam was concave along its long axis. The walls of the beam were thicker than its middle. Material is deposited faster where the density of the electric field is higher – in this case, at the edges of the mould. The difference is small, but the long process enlarged the effect. Bending of the cantilever caused by internal stresses was not observed.

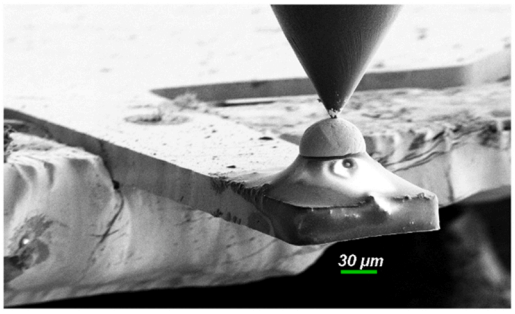

Fig. 7. Calibration of the stiff probe with the ball as tip.

Table 2
Results of the friction coefficient measurement with the probe with the ball as the tip.

	Substrate type			
	Silicon	Steel	Titanium	TiC
Ra roughness [nm]	0.69	3.7	1.46	2.17
COF – 5 mN load	0.395 ± 0.041	0.201 ± 0.021	0.228 ± 0.023	0.342 ± 0.035

The stiffness, LFCC, and sensitivity were calibrated as described previously. An overview of the stiffness calibration process is shown in Fig. 7. The obtained stiffness of the probe was 2846 ± 66 N/m, the sensitivity was 1091 nm/V, and the LFCC was 54 mN/V.

3.4. Friction experiments with a glued ball tip

The probe described in the previous paragraphs was used for the measurement of friction on four different samples: silicon wafer, polished steel, polished titanium, and TiC (titanium carbide) obtained by PVD (Plasma Vapour Deposition). As mentioned before, the tip was made of soda-lime glass. The roughness of the samples was measured on 20 μm long profiles extracted from a levelled image. The COF was measured using the lateral force mode. A single line of measurement was 20 μm long, and the speed of the tip was 20 μm/s. The normal force was set to 5 mN. 20 lines were measured in a single experiment, and it was repeated 3 times on various areas of the samples. The results of both the roughness and friction are shown in Table 2. The uncertainty of the results is calculated as a combination of the uncertainty of determination of the probe parameters and the standard deviation of the obtained results.

It is worth noting that a similar experiment was performed by Yoon et al. [40]. However, the main difference between our approach and their work is the use of AFM instead of a micro tribometer. In their experiments, the COF between the soda lime glass ball with a diameter of 250 μm and the silicon substrate was close to 0.3 for a 5 mN load. This value is close to the here obtained value, which validates the results obtained in this preliminary study. Unfortunately, to the best of our knowledge, there are no other publications testing such friction pairs in this scale.

3.5. Changing the shape of the imaging tip

Our method is capable of producing AFM probes with any convex shape. In this paper, the tests of reproduction of custom shaped moulds

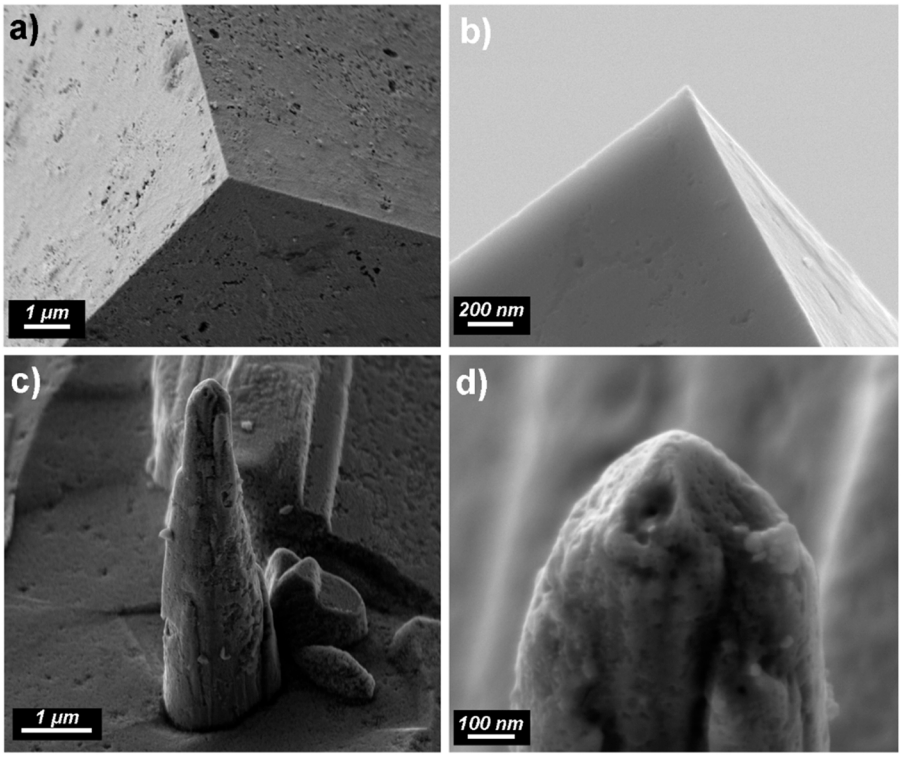

Fig. 8. Measuring tips made with various indenter tips. a) top view of cube corner tip, b) side view of cube corner tip, c) side view of the custom tip, d) close-up of the custom tip.

were performed as the last experiment. Cube-corner and custom shaped high aspect ratio tips were used, as described in Section 2.4. In both cases, the electroplated material exactly recreated the shape of the indentation tip. The obtained tips are shown in Fig. 8. The measured radius of the cube corner tip was smaller than 40 nm, and the radius of the custom high-aspect-ratio tip was smaller than 50 nm.

4. Discussion

Discussion of the results described in the paper can be divided into three parts. The first part is the novel method of fabrication in relation to other methods. The second part is the advantages and disadvantages of the novel probes as a tool. Lastly, the results of the conducted tribological experiments, although sparse, are analyzed and discussed.

4.1. Method of fabrication

The method of fabrication proposed by us changes the paradigm of AFM probe fabrication and design. Currently, only silicon probes are widely available on the market. Metal probes are available as a special order. The methods of fabrication proposed by other researchers did not lead to commercialisation but can be used for small-scale production. Most of them use silicon as a substrate. [21–23] Tips are created either by etching silicon to create a pyramid-shaped mould or by some complicated methods, such as FIB milling [15], gluing of wires [17], or multistep deposition. Changing the substrate from the most common silicon to copper allows direct use of electrochemistry, and no additional sacrificial layers are required. Therefore, it decreases the costs of fabrication, i.e., copper is much cheaper than silicon and electroplating is cheaper than PVD. It allows for the creation of probes from nearly any metal. Most metals and even some alloys can be electroplated. Additionally, the thickness of the probe can be precisely controlled with only one parameter, the time of plating. Therefore, the creation of both thin and thick probes is possible, as showcased above. The use of indentation for moulds makes it easier to create custom-shaped tips. Even if FIB milling is required to create an indentation tip for moulding, then it could be used to create multiple probes, while traditionally, every probe would have to be milled [41].

The used substrate poses new challenges that can be regarded as minor disadvantages of the method. The preparation of the substrates is long, as it must be polished to a mirror finish. Fortunately, this task can be easily automated just like in the case of silicon wafers. Etching the substrate requires the use of a substantial amount of chemicals and results in the creation of a large volume of chemical waste. On the other hand, the low cost of these materials outweighs the drawbacks.

In general, the conducted experiments proved the concept of fabrication method as valid . All steps of the process worked well. Although some minor issues with the final probes are visible, it is mostly due to the used equipment and not the method. For example, the misalignment of the tip visible in Fig. 5a was caused by drift in the indentation device. Such problems are easily solvable and had no influence on the usability of the fabricated probes. Devices already present in the laboratory and the scale of production were limiting factors here. The yield of devices in low-scale production is expected to be low.

4.2. Probes

The resonant frequency of the probe used in the test was smaller than expected. Similarly, the stiffness was around 2 times smaller than the theoretical value. Although unwanted, this is a common problem with all AFM probes [42], as small imperfections and deviations in size lead to a big change in the properties. This was most probably caused by irregularities in the shape of the beam, the presence of a measuring tip, small dust particles on the beam, the small inhomogeneity and the presence of elements other than nickel in the deposited material [43]. Common silicon probes have an expected stiffness with an error even larger than 100%, and due to the irregular cross-section it is hard to precisely determine in AFM [44]; therefore, a 50% deviation for the all-metal probe is reasonable and certainly can be limited by fine-tuning all processes.

Attaching a sphere to the metal cantilever was easier than attaching it to a silicon probe. Metal probes are less brittle and larger (than a Si-probe with the same stiffness), which makes them more durable. In both cases, probes were heavily strained during glueing, but the elasticity of the metal allowed it. Their high durability allowed to move swiftly and user of AFM did not have to worry about damaging the probe. No additional manipulator was required.

Friction experiments were conducted with two probes with widely different stiffnesses and therefore with normal load in the range of 2 orders of magnitude. In the literature, various forces are referred to as "high-load", ranging from 1 μN [45,46] up to 150 μN [47]. In this publication, experiments were conducted with forces in the range of 10–50 μN and also 5 mN. Even a lower range qualifies as a "high-load", while 5 mN load was previously hard to achieve in AFM.

A practical example can be given for the case of experiments performed by Wang et. al. [48] in which they tested the tribological behaviour of the nanodot-patterned surface. For experiments with high loads of 500 μN, they used a TriboIndenter, which is a precise nano-indentation device with possible lateral movement. Another example can be given in the by Karrupiah et. al. [49] in which they measured friction on mica. For loads under 50 μN, they used AFM, while for loads up to 8 mN, they used a micro tribometer. The use of high-stiffness probes would allow all the described experiments to be conducted with AFM. A single device could be used for both imaging and scratching. This would simplify and speed up the work while providing the same working conditions. Great results in using AFM with millinewton-range forces were reported by Garabedian et. al. [13]. In their paper probes were modified by attaching metal spheres at various places on the cantilever, which allowed a 5 mN normal load to be exerted in experiments. Although successful, this method also has some disadvantages when compared to the here described procedure. Spheres had to be attached by a custom micromanipulator, while here described metal probes allow glueing directly with the AFM. Moreover, the same modifications can be done with an ultra-stiff metal probe, increasing effective stiffness by another order of magnitude. Here described probes are a great base for attaching spheres as shown in the example in Fig. 3d). The ball with 300 μm diameter could not be attached to common silicon probe, as it would be much larger than the cantilever. Epoxy would either have not enough contact with the ball to allow ultra-high-load experiments or completely cover the cantilever and render it useless.

With our novel method, the stiffness can be fine-tuned and even higher values are possible. These results show that our probes can be used in previously impossible experiments. They will allow tribological experiments between various materials on the boundary between the nano-, micro-, and mesoscale in one device – an atomic force microscope. Previously, experiments with AFM were limited by the materials (Si, Si_3N_4) and parameters (probe stiffness 0.01–100 N/m).

Moreover, all-metal probes fabricated as described can be used in other kinds of experiments, including magnetic (nickel is ferromagnetic) [50,51] and electrical modes (as metals conduct electricity). Such experiments are planned in the near future.

The biggest disadvantage of the all-metal probes used in the experiments is the shape of the tip. As a Vickers indentation tip was used for making moulds, the tip angle is large. Therefore, these probes cannot be used for measuring structures with a high aspect ratio. Similarly, the tip has a large radius of curvature. The experiment with other indentation tips for moulds was successful, as the electrodeposited material filled them and exactly reflected the shape. The radius of these tips was still larger than that of a common silicon probe but comparable to probes with a metal coating. Also, FIB milling of indenters could be optimised for the tip radius rather than the aspect ratio.

Last, a less obvious advantage of all-metal probes is their usability. Both the beam and base have vertical sidewalls. This makes it easier to grab them with tweezers. It is also easier to estimate the properties of beams with a rectangular cross-section than silicon beams with a trapezoidal cross-section.

4.3. Results obtained with the novel probes

Firstly, the topographical image of the calibration sample confirmed the SEM observation of the probe. The shape of the tip is regular and symmetrical. The obtained image of the calibration sample is clean, but on the edges of the structure, the effect of a large radius of curvature and large tip-angle is visible. They are not as sharp as those imaged with silicon probes. Nonetheless, the obtained image showed the proper dimensions of the structure.

Tribological experiments conducted in this study were meant to showcase the capabilities of the probes rather than being a thorough study. They can be treated as a prelude to an extensive investigation of friction across the scales with the help of AFM. For the all-metal nickel probe, the decrease in the coefficient of friction was observed with the increase in load. This behaviour was similar for all investigated materials and is in good agreement with the theory of friction coefficient based on the Hertz theory. [52] Furthermore, nickel and copper exhibited nearly the same values despite being different materials and having different roughnesses. Results obtained by classical silicon probe show, as expected, different behaviour. COF also changes depending on normal load, but differently for each material-pair. On silicon COF increases with load, on nickel COF is going slightly down and then slightly up, and on copper it also goes slightly down to then increase dramatically. It is worth noting that COF for nickel probe on silicon and for silicon probe on nickel is different. Right now this difference is tentatively attributed to the difference in contact area caused by tip shape and sample roughness. To clearly determine the nature of these changes more thorough experiment must be conducted.

For the probe with the soda-lime glass ball tip, the results also show interesting values of COF. Silicon had the highest value, probably due to the high adhesion and high real contact area (low silicon roughness). On the other hand, for the all-metal probe, the silicon substrate had the smallest COF due to the partial incompatibility, in the adhesive sense, between silicon and nickel [53]. It should be noted that the uncertainty of the results was around 10% for both types of probes. Hence, the calibration was performed well.

The materials tested in both scales were different; therefore, the results cannot be directly compared, but they can show the direction for further research. The obtained results are strong evidence that the scale of the experiments plays an important role in the friction experiments. This is also supported by many existing scientific publications. Experiments across the scales would help validate existing models for friction [30,54] and help create new ones, including thermodynamic behaviour [55]. This is also crucial in the case of MEMS (micro-electro-mechanical systems) design, working principle, and reliability [56,57].

For a deep understanding of the behaviour of materials, a meticulous experimental investigation must be performed that takes into account all of the conditions: material pair, load, roughness, speed, contact area [37,38]. The probes described in this paper will allow control over these parameters over a wide range in one device (i.e., AFM), opening new possibilities in tribology.

5. Conclusion

A novel method for the production of all-metal AFM probes was proposed and then conducted to prepare a series of nickel probes with various stiffnesses. The obtained probes had good reflectivity of the laser beam and were characterised by a high-quality frequency response. These probes were successfully used for experiments in AFM, including topography and friction measurements. Both the method of fabrication and the metal probes have many advantages over classical probes. This novel approach can broaden the scope of AFM use by providing probes with a wider range of stiffnesses and more diverse tip shapes and that are made of previously unavailable materials.

Table A1
Stiffness determined by different methods.

	Used method of determination			
	Geometrical	Frequency (thickness as unknown)	Frequency (length as unknown)	Nanoindentation tester
Stiffness [N/m]	28.8 ± 2.4	12.4 ± 3.6	18.9 ± 3.8	20.88 ± 1.36

Statement of originality

As corresponding author, I Dariusz Jarząbek, hereby confirm on behalf of all authors that:

1) The paper has not been published previously, that it is not under consideration for publication elsewhere, and that if accepted it will not be published elsewhere in the same form, in English or in any other language, without the written consent of the publisher.
2) The paper does not contain material which has been published previously, by the current authors or by others, of which the source is not explicitly cited in the paper.

Declaration of Competing Interest

The authors declare the following financial interests/personal relationships which may be considered as potential competing interests: Michal Milczarek reports financial support was provided by National Centre for Research and Development. Dariusz Jarzabek reports financial support was provided by National Centre for Research and Development. Piotr Jenczyk reports financial support was provided by National Centre for Research and Development.

Data availability

Data will be made available on request.

Acknowledgements

This work has been conducted for the UWIPOM2 project, which received funding from the European Union's Horizon 2020 research and innovation programme under grant agreement No 857654. This research was also partially supported by the National Centre for Research and Development (Poland) grant TANGO III 425497/NCBR/2019.

We would like to thank our colleagues, Marcin Michałowski for providing micro balls and inspiration for the high load experiments, and Tomasz Wojciechowski for help with the preliminary photolithography experiments.

Appendix 1. On the determination of the normal stiffness of probes

Below, description of the three methods that can be used for the determination of the normal stiffness of probes are given: geometrical, indirect from resonant frequency, and direct.

In the geometrical approach, the stiffness is calculated based only on the measured dimensions of the cantilever using the following formula [33]:

$$k = \frac{P}{\delta} = \frac{\frac{bh^3}{4}E}{l^3} = \frac{Ebh^3}{4l^3} \tag{A.1}$$

in which: k – stiffness, P – force on the tip, δ – deflection of the tip, b – width of the beam, h – thickness of the beam, l – length of the beam from base to tip, E – Young's modulus.

In the indirect approach, one of the dimensions was treated as an unknown, and it was subsequently calculated based on the resonance frequency of the probe determined by AFM [34]. The uncertainty of the length and thickness has the greatest influence on the result; therefore, it is most advantageous to determine them from a precisely determined frequency. The first resonant frequency of a cantilever beam is given by the following formula:

$$f = \frac{1,875^2}{2\pi l^2}\sqrt{\frac{EI}{\rho A}} = \frac{1,875^2}{2\pi}\frac{1}{l^2}\sqrt{\frac{E\frac{bh^3}{12}}{\rho bh}} = \frac{1,875^2}{2\pi}\sqrt{\frac{1}{12}}\frac{1}{l^2}\sqrt{\frac{Ebh^3}{\rho bh}} = \beta\frac{h}{l^2}\sqrt{\frac{E}{\rho}} \tag{A.2}$$

in which: f – frequency, β – constant, E – Young's modulus, I – second moment of inertia of the beam cross-section, ρ – density of the material, A – area of the beam cross-section, b – width of the beam, h – thickness of the beam, l – length of the beam from the base to tip.

This formula can be transformed to calculate the thickness or length of the beam as follows:

$$h = \frac{1}{\beta}\sqrt{\frac{\rho}{E}}fl^2 \tag{A.3}$$

$$l = \sqrt{\beta\frac{h}{f}\sqrt{\frac{E}{\rho}}} \tag{A.4}$$

As above, the calculated dimension can then be substituted into formula (1) to determine the stiffness of the probe.

The direct method uses a nanoindentation device. The probe is mounted as a sample, and a flat-ended indenter-tip is used to push against the probe tip. It can be performed using in-situ SEM to allow accurate positioning of the indenter. The force used for the calibration should be in the same range as that used in the experiments. It is a precise method, as the nanoindenter directly measures the force and deflection.

The stiffness obtained from each method is summarised in Table A1. The calibrated probe is a nickel cantilever with dimensions of 105 μm x 590 μm x 10.4 μm. The same probe is used for the experiments in the paper. For the direct method with the nanoindenter, the Alemnis device was used, and procedure was repeated 6 times with various displacements.

References

[1] Binnig Quate. Gerber atomic force microscope. Phys Rev Lett 1986;56:930–3. https://doi.org/10.1103/PhysRevLett.56.930.

[2] Voigtländer B. Atomic force microscopy. Cham: Springer International Publishing; 2019. https://doi.org/10.1007/978-3-030-13654-3.

[3] Morita S, Giessibl FJ, Wiesendanger R, editors. Noncontact atomic force microscopy. Heidelberg: Springer Berlin Heidelberg; 2009. https://doi.org/10.1007/978-3-642-01495-6.

[4] Reichelt M, Cappella B. Atomic force microscope study of friction at the submicron-scale during tribotests with self-mated steel. J Tribol 2022:144. https://doi.org/10.1115/1.4054251.

[5] Wubetu GA. Nanoscale friction force on thin films of polymer blends and silane layers matrix. Tribol Int 2023;177:107984. https://doi.org/10.1016/j.triboint.2022.107984.

[6] McGuiggan PM, Zhang J, Hsu SM. Atomic force microscope study of friction at the submicron-scale during tribotests with self-mated steel. Tribol Lett 2001;10:217–23. https://doi.org/10.1023/A:1016692704748.

[7] Mathieson D, Beerschwinger U, Yang SJ, Reuben RL, Taghizadeh MR, Eckert S, et al. Effect of progressive wear on the friction characteristics of nickel LIGA processed rotors. Wear 1996;192:199–207. https://doi.org/10.1016/0043-1648(95)06802-3.

[8] Kim DW, Lee JH, Kim JK, Jeong U. Material aspects of triboelectric energy generation and sensors. NPG Asia Mater 2020;12(1):1–17. https://doi.org/10.1038/s41427-019-0176-0.

[9] Wu C, Wang AC, Ding W, Guo H, Wang ZL. Triboelectric nanogenerator: a foundation of the energy for the new era. Adv Energy Mater 2019;9:1802906. https://doi.org/10.1002/AENM.201802906.

[10] Gacka E, Kunicki P, Sikora A, Bogdanowicz R, Ficek M, Gotszalk T, et al. Focused ion beam-based microfabrication of boron-doped diamond single-crystal tip cantilevers for electrical and mechanical scanning probe microscopy. Measurement 2022:188. https://doi.org/10.1016/J.MEASUREMENT.2021.110373.

[11] Samaan M, Ekinci H, Dey R, Zhu X, Pushin D, Cui B. Fabrication of high aspect ratio atomic force microscope probes using focused ion beam milled etch mask. Microelectron Eng 2023;267–268:111909. https://doi.org/10.1016/J.MEE.2022.111909.

[12] Cespedes O, Luu A, Rhen F, Coey J. Fabrication of magnetic force microscopy tips via electrodeposition and focused ion beam milling. IEEE Trans Magn 2008;44:3248–51. https://doi.org/10.1109/TMAG.2008.2002866.

[13] Garabedian NT, Khare HS, Carpick RW, Burris DL. AFM at the macroscale: methods to fabricate and calibrate probes for millinewton force measurements. Tribol Lett 2019;67:21. https://doi.org/10.1007/s11249-019-1134-2.

[14] Bhushan B, Palacio M, Kwak KJ. Thermally-treated Pt-coated silicon AFM tips for wear resistance in ferroelectric data storage. Acta Mater 2008;56:4233–41. https://doi.org/10.1016/j.actamat.2008.04.052.

[15] Akiyama K, Eguchi T, An T, Fujikawa Y, Yamada-Takamura Y, Sakurai T, et al. Development of a metal-tip cantilever for noncontact atomic force microscopy. Rev Sci Instrum 2005. https://doi.org/10.1063/1.1865812.

[16] Tay ABH, Thong JTL. Fabrication of super-sharp nanowire atomic force microscope probes using a field emission induced growth technique. Rev Sci Instrum 2004;75:3248–55. https://doi.org/10.1063/1.1791321.

[17] Walke P, Fujita Y, Peeters W, Toyouchi S, Frederickx W, De Feyter S, et al. Silver nanowires for highly reproducible cantilever based AFM-TERS microscopy: towards a universal TERS probe. Nanoscale 2018;10:7556–65. https://doi.org/10.1039/C8NR02225A.

[18] Michałowski M, Łuczak S. AFM cantilevers with spherical tip of millimeter size. J Micromech Microeng 2019;29:017002. https://doi.org/10.1088/1361-6439/aaee56.

[19] Rodriguez RD, Anne A, Cambril E, Demaille C. Optimized hand fabricated AFM probes for simultaneous topographical and electrochemical tapping mode imaging. Ultramicroscopy 2011;111:973–81. https://doi.org/10.1016/j.ultramic.2011.02.001.

[20] Kolchuzhin VA, Sheremet E, Bhattacharya K, Rodriguez RD, Paul SD, Mehner J, et al. Mechanical properties and applications of custom-built gold AFM cantilevers. Mechatronics 2016;40:281–6. https://doi.org/10.1016/j.mechatronics.2016.05.015.

[21] Zou J, Wang X, Bullen D, Ryu K, Liu C, Mirkin CA. A mould-and-transfer technology for fabricating scanning probe microscopy probes. J Micromech Microeng 2004;14:204–11. https://doi.org/10.1088/0960-1317/14/2/006.

[22] Luber EJ, Olsen BC, Ophus C, Radmilovic V, Mitlin D. All-metal AFM probes fabricated from microstructurally tailored Cu–Hf thin films. Nanotechnology 2009;20:345703. https://doi.org/10.1088/0957-4484/20/34/345703.

[23] Rasmussen JP, Tang PT, Sander C, Hansen O, Moller P. Fabrication of an all-metal atomic force microscope probe. In: Proceedings of the international solid state sensors and actuators conference (Transducers '97), vol. 1, IEEE; 2002, pp. 463–6. ⟨https://doi.org/10.1109/SENSOR.1997.613686⟩.

[24] Kölling S, Hantschel T, Vandervorst W. Conductive diamond probes with electroplated holder chips. Microelectron Eng 2007;84:1178–81. https://doi.org/10.1016/J.MEE.2007.01.047.

[25] Hantschel T, Pape U, Slesazeck S, Niedermann P, Vandervorst W. In: Vladimirsky Y, Coane PJ, editors. Mounting of molded AFM probes by soldering; 2000. p. 62. https://doi.org/10.1117/12.395613.

[26] Yu Q, Qin G, Darne C, Cai C, Wosik W, Pei S-S. Fabrication of short and thin silicon cantilevers for AFM with SOI wafers. Sens Actuators A Phys 2006;126:369–74. https://doi.org/10.1016/j.sna.2005.10.019.

[27] Chemical Etching and Patterning of Copper, Silver, and Gold Films at Low Temperatures; n.d. ⟨https://doi.org/10.1149/2.0111501jss⟩.

[28] Lin S. Finishing (USA) TW-P and S, 1991 undefined. The effect of additives on the internal stress of nickel deposits from watts baths. StercOrg n.d.

[29] Jenczyk P, Gawrońska M, Dera W, Chrzanowska-Giżyńska J, Denis P, Jarząbek DM. Application of SiC particles coated with a protective Ni layer for production of Ni/SiC co-electrodeposited composite coatings with enhanced tribological properties. Ceram Int 2019;45:23540–7. https://doi.org/10.1016/j.ceramint.2019.08.063.

[30] Michałowski M. Simulation model for frictional contact of two elastic surfaces in micro/nanoscale and its validation. Nanotechnol Rev 2018;7:355–63. https://doi.org/10.1515/NTREV-2018-0075/MACHINEREADABLECITATION/RIS.

[31] Korayem MH, Zakeri M. Sensitivity analysis of nanoparticles pushing critical conditions in 2-D controlled nanomanipulation based on AFM. Int J Adv Manuf Technol 2009;41:714–26. https://doi.org/10.1007/S00170-008-1519-0/METRICS.

[32] Korayem MH, Sadeghzadeh S, Rahneshin V. A new multiscale methodology for modeling of single and multi-body solid structures. Comput Mater Sci 2012;63:1–11. https://doi.org/10.1016/J.COMMATSCI.2012.05.059.

[33] Tortonese M, Kirk M. In: Michalske TA, Wendman MA, editors. Characterization of application-specific probes for SPMs. vol. 3009; 1997. p. 53–60. https://doi.org/10.1117/12.271229.

[34] Sader JE, Chon JWM, Mulvaney P. Calibration of rectangular atomic force microscope cantilevers. Rev Sci Instrum 1999;70:3967–9. https://doi.org/10.1063/1.1150021.

[35] Grutzik SJ, Gates RS, Gerbig YB, Smith DT, Cook RF, Zehnder AT. Accurate spring constant calibration for very stiff atomic force microscopy cantilevers. Rev Sci Instrum 2013;84:113706. https://doi.org/10.1063/1.4832978.

[36] Dziekoński C, Dera W, Jarząbek DM. Method for lateral force calibration in atomic force microscope using MEMS microforce sensor. Ultramicroscopy 2017;182:1–9. https://doi.org/10.1016/j.ultramic.2017.06.012.

[37] Bhushan B, editor. Nanotribology and nanomechanics. Cham: Springer International Publishing; 2017. https://doi.org/10.1007/978-3-319-51433-8.

[38] Bhushan B. Principles and applications to tribology. The Atrium, Southern Gate, Chichester, West Sussex, PO19 8SQ, UK: John Wiley & Sons, Ltd; 2013. https://doi.org/10.1002/9781118403020.

[39] Grzywacz H, Milczarek M, Jenczyk P, Dera W, Michałowski M, Jarząbek DM. Quantitative measurement of nanofriction between PMMA thin films and various AFM probes. Measurement 2021;168:108267. https://doi.org/10.1016/j.measurement.2020.108267.

[40] Yoon ES, Singh RA, Oh HJ, Kong H. The effect of contact area on nano/micro-scale friction. Wear 2005;259:1424–31. https://doi.org/10.1016/J.WEAR.2005.01.033.

[41] Eifert A, Mizaikoff B, Kranz C. Advanced fabrication process for combined atomic force-scanning electrochemical microscopy (AFM-SECM) probes. Micron 2015;68:27–35. https://doi.org/10.1016/J.MICRON.2014.08.008.

[42] Sader JE, Borgani R, Gibson CT, Haviland DB, Higgins MJ, Kilpatrick JI, et al. A virtual instrument to standardise the calibration of atomic force microscope cantilevers. Rev Sci Instrum 2016;87:093711. https://doi.org/10.1063/1.4962866.

[43] Kolonits T, Jenei P, Péter L, Bakonyi I, Czigány Z, Gubicza J. Effect of bath additives on the microstructure, lattice defect density and hardness of electrodeposited nanocrystalline Ni films. Surf Coat Technol 2018;349:611–21. https://doi.org/10.1016/J.SURFCOAT.2018.06.052.

[44] Sader JE, Borgani R, Gibson CT, Haviland DB, Higgins MJ, Kilpatrick JI, et al. A virtual instrument to standardise the calibration of atomic force microscope cantilevers. Rev Sci Instrum 2016;87:093711. https://doi.org/10.1063/1.4962866.

[45] Liu SW, Wang HP, Xu Q, Ma TB, Yu G, Zhang C, et al. Robust microscale superlubricity under high contact pressure enabled by graphene-coated microsphere. Nat Commun 2017;8:1–8. https://doi.org/10.1038/ncomms14029.

[46] Gulbiński W, Suszko T, Pailharey D. High load AFM friction and wear experiments on V2O5 thin films. Wear 2003;254:988–93. https://doi.org/10.1016/S0043-1648(03)00304-1.

[47] Bhushan B, Sundararajan S. Micro/nanoscale friction and wear mechanisms of thin films using atomic force and friction force microscopy. Acta Mater 1998;46:3793–804. https://doi.org/10.1016/S1359-6454(98)00062-7.

[48] Wang H, Premachandran Nair R, Zou M, Larson PR, Pollack AL, Hobbs KL, et al. Friction study of a Ni nanodot-patterned surface. Tribol Lett 2007;28:183–9. https://doi.org/10.1007/S11249-007-9263-4/TABLES/1.

[49] Kanaga Karuppiah KS, Bruck AL, Sundararajan S. Evaluation of friction behavior and its contact-area dependence at the micro- and nano-scales. Tribol Lett 2009;36:259–67. https://doi.org/10.1007/S11249-009-9483-X/TABLES/3.

[50] Bauer P, Bochem HP, Leinenbach P, Memmert U, Schelten J. Magnetic refinement of tips for magnetic force microscopy. Scanning 1996;18:374–8. https://doi.org/10.1002/sca.1996.4950180508.

[51] Cespedes O, Luu A, Rhen F, Coey J. Fabrication of magnetic force microscopy tips via electrodeposition and focused ion beam milling. IEEE Trans Magn 2008;44:3248–51. https://doi.org/10.1109/TMAG.2008.2002866.

[52] Bhushan B. Principles and applications of tribology. vol. 98; 1976. https://doi.org/10.1115/1.3452952.

[53] Rabinowicz E. Friction and wear of materials. 2nd ed. 1995. p. 336.

[54] Białas M, Maciejewski J, Kucharski S. Friction coefficient of solid lubricating coating as a function of contact pressure: experimental results and microscale modeling. Contin Mech Thermodyn 2021;33:1733–45. https://doi.org/10.1007/S00161-021-00999-0/FIGURES/11.

[55] Temizer I. Sliding friction across the scales: thermomechanical interactions and dissipation partitioning. J Mech Phys Solids 2016;89:126–48. https://doi.org/10.1016/J.JMPS.2016.01.012.
[56] Tambe NS, Bhushan B. Scale dependence of micro/nano-friction and adhesion of MEMS/NEMS materials, coatings and lubricants. Nanotechnology 2004;15:1561. https://doi.org/10.1088/0957-4484/15/11/033.
[57] Komvopoulos K. Adhesion and friction forces in microelectromechanical systems: mechanisms, measurement, surface modification techniques, and adhesion theory. J Adhes Sci Technol 2012;17:477–517. https://doi.org/10.1163/15685610360554384.